# Investigation of CTF void fraction prediction by ENTEK BM experiment data

Hoang Minh Giang[1], Hoang Tan Hung[1], Nguyen Phu Khanh[2]

[1] Nuclear Safety Center, Institute for Nuclear Science and Technology
[2]Hanoi University of Science and Technology

**Abstract**

Recently, CTF, a version of COBRA-TF code is reviewed to validate its simulation models by several experiments such as Castellana 4x4 rod bundle, EPRI 5x5 bundle tests, PSBT bundle tests and TPTF experiment. These above experiments provide enthalpy, mass flux (Castellana), temperature (EPRI) and void fraction (PSBT, TPTF) at exit channel only. In order to simulate PWR rod bundle flow behavior, it is necessary to review CTF with more experiment in high pressure condition and it is found that the ENTEK BM facility is suitable for this purpose. The ENTEK BM facility is used to simulate Russia RBMK and VVER rod bundle two phase flow with pressure at 3 and 7 MPa and it gives measured void fraction distribution along the channel. This study focus on two points: (a) accuracy assessment between CTF's void fraction distribution predictions versus experiment void fraction distributions and (b) investigation of void fraction prediction uncertainty from propagation of input deviations caused by measured accuracy.

## 1. Introduction

COBRA-TF is released in many versions and is widely used to investigate vertical channel flow. A study of COBRA-TF void fraction recalculation using experimental data of both the OECD/NRC BFBT benchmark and in-house tests in AREVA NP's KATHY loop is presented in [1]. The Ref.1 introduces several correlations to correct void fraction based on experiment void fraction derived from measured density. Another assessment of the COBRA-TF performance for the prediction of sub cooled boiling conditions in heated rod bundles with Light Water Reactors operating conditions is reported in [2]. The assessment in the Ref. [2] consists of two parts: (a) a comparison of COBRA-TF predictions to data from three heated bundle experiments and (b) an evaluation of the physics models and constitutive relations within COBRA-TF. Some conclusions from this report are related to fluid temperature distribution and wall temperature distribution based on EPRI 5x5 rod bundle tests. For the void fraction study, it is shown in Ref. [2] that COBRA-TF and COBRA-EN predict similar in the locations within the channel at which the flow quality is greater than zero. Furthermore, COBRA-TF predicts none zero void at near channel inlet, even when the flow quality is predicted to be zero. The Ref. [3] shows the study of CTF void fraction prediction for PSBT single channel exercises. It can be seen that the CTF predictions stay within the error bound of 0.1 void (the CT scanner cross section average void measurements were specified as an uncertainty of 0.03). From the Ref. [3], it is observed a tendency that CTF over predict the vapor generation rate, which is due the utilized interfacial drag modeling in CTF. The study presented in [4] do not mention directly about CTF void fraction prediction, but it is found that CTF is over predicting the liquid enthalpy due to an incorrect partitioning of heat input to the fluid. Thus, CTF may be considered as inaccurate prediction tool for some of the flow quantities in the experiments such as Castellana 4x4 rod bundle, EPRI 5x5 cases and standard 17 x 17 PWR rod bundle. So that it is necessary to validate CTF void fraction prediction with an experiment in high pressure condition to verify its accuracy and the ENTEK BM tests it is suitable for this study. CTF, a COBRA-TF version with inhomogeneous models of two phase flow, is developed by Pennsylvania State University and is transferred to Vietnam Agency for

Radiation and Nuclear Safety (VARANS) through bilateral cooperation. Therefore, CTF is considered as a tool at sub channel scale to investigate core thermal hydraulics by technical support organizations (TSOs). This study focuses on two points: (a) accuracy assessment between CTF's void fraction predictions versus experiment distributions along the channel and (b) uncertainty of void fraction prediction due to propagation of input uncertainty caused by measured accuracy.

## 2. Brief of CTF models for evaporation and condensation

*Evaporation and condensation induced by thermal phase change*

The CTF model includes nine conservation equations and three fields: liquid, vapor and entrained liquid drop. The various forms of conservation equations and its closure models are presented [3,5 ]. There are two different types of flow regime maps: "normal wall" map and "hot wall" map. The normal wall map is used when the maximum wall surface temperature ($T_w$,) in a given computational mesh cell is below the critical heat flux temperature, $T_{crit}$. Then a part of wall adjacent to this mesh cell is expected to be fully wetted. The normal wall flow regime map includes the following flow regimes: small bubble; small-to-large bubble (slug); churn/turbulent; and annular/mist. The hot-wall regime map includes: inverted annular, inverted slug, dispersed droplet, falling film that happen in case of a heated surface in the analysis volume is greater than the CHF temperature. In the sub cooled region, Newton's law of cooling is used to characterize heat transfer between solid surfaces and the fluid:

$$q_w''' = h_c(T_w - T_l)\frac{A_S}{A_x \Delta X} \tag{1}$$

Whenever heat from the wall is transferred to liquid, liquid enthalpy increases and the phase change which is expressed via volumetric mass flow rate, Γ''', is calculated by subtracting condensation terms (sub-cooled liquid and vapor terms) from evaporation terms (superheated liquid and vapor) terms:

$$\Gamma''' = \left[\frac{A'''_{int,shl}\ h_{i,shl}}{(h_{g,sat}-h_{l,sat})C_{pl}}\left|h_l - h_{l,sat}\right| + \frac{A'''_{int,shv}h_{i,shv}}{(h_{g,sat}-h_{l,sat})C_{pv}}\left|h_g - h_{g,sat}\right|\right] - \left[\frac{A'''_{int,scl}h_{i,scl}}{(h_{g,sat}-h_{l,sat})C_{pl}}\left|h_l - h_{l,sat}\right| + \frac{A'''_{int,scv}h_{i,scv}}{(h_{g,sat}-h_{l,sat})C_{pv}}\left|h_g - h_{g,sat}\right|\right] \tag{2}$$

*Evaporation and condensation induced by turbulent mixing and void drift*

Another phenomenon that can cause phase change is turbulence. The CTF's turbulent mixing and void drift uses a simple turbulent-diffusion model by calculating the lateral velocity from sub channel to sub channel. Based on the turbulent mixing model, the mass flux exchange of phase (k) ($\dot{m}_k^{TM}$) induced by sub channel (i) and (j) can be defined as:

$$\dot{m}_k^{TM} = \beta_{TP}\frac{\bar{G}}{\bar{\rho}}\left(\alpha_{kj}\rho_{kj} - \alpha_{ki}\rho_{ki}\right) \tag{3}$$

The mass exchange ( $\dot{m}_k^{VD}$ ) due to drift model is obtained:

$$\dot{m}_k^{VD} = \beta_{TP}\frac{\bar{G}}{\bar{\rho}}\left(\alpha_{kjEQ}\rho_{kjEQ} - \alpha_{kiEQ}\rho_{kiEQ}\right)S_k\Delta X \tag{4}$$

In the formulas (3) and (4), $\beta_{TP}$ , $\bar{G}$ , $S_k$ and $\Delta X$ are Beus' correlation for two-phase turbulent mixing coefficient [7], average mass flux between adjacent sub-channels, gap between channels (i) (j) and mesh-cell axial height, respectively.

## 3. Short brief of ENTEK BM facility modeling

*ENTEK BM facility*

As mentioned in [6], Figure 1 provides a vertical and cross-section view of the test section which is also called as Heated Release Zone (HRZ). For the cross section view, the diameters are shown in millimeters. The HRZ contains a 7-rod bundle made by stainless steel (X18H10T). All the rods are hollow with outer diameter of 13.5 mm, 1.25 mm wall thickness, and 7 m length. The bundle is contained within a stainless steel pressure tube (80 mm outer diameter and 5 mm wall thickness) with inner diameter of 49 mm and 10.5 mm wall thickness. The coolant flow area is $8.84\times10^{-4}m^2$ and the hydraulic diameter is 7.84 mm. There are 20 honeycomb-type pin spacing grids along the length of the HRZ, starting 30 mm from the beginning of the HRZ and repeated every 350 mm. Thus, these spacing grids are similar to the spacers in the RBMK-1000 with a hydraulic loss coefficient of 0.4 based on measurements.

The uncertainties of the measurements for each parameter are following for all tests:

- Pressure at HRZ outlet: ±1.5 %;
- Coolant mass flow rate : ±0.0018 kg/s;
- Coolant temperature at HRZ inlet: ±1 K;
- Electrical power: ±2 kW;
- Void fraction: ±0.03; (void is calculated rather than measured).

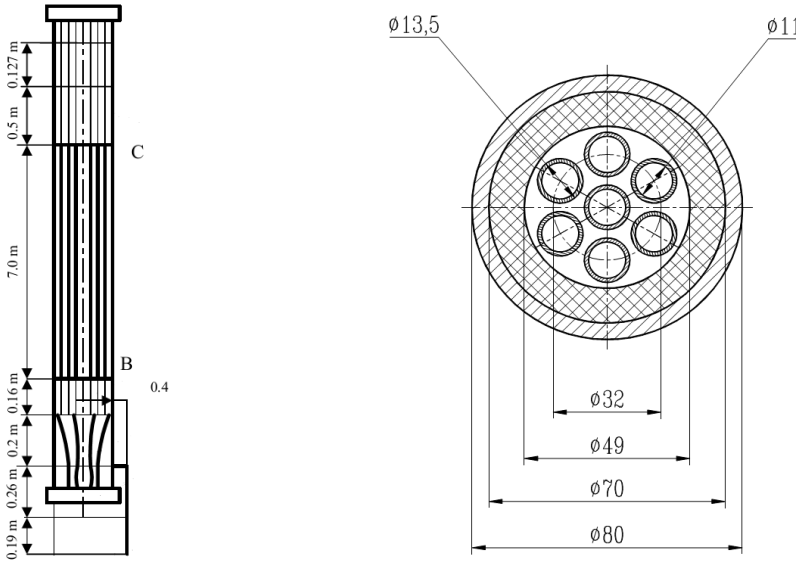


Figure 1 Test Section (Heat Release Zone, φ is diameter in mm) with vertical and cross section view [6].

The test section is also called Heat Release Zone is illustrated from point "B" to point "C" in the Figure 1. Measurement readings were obtained at 10 axial locations (i.e., 0.385, 0.948, 1.573, 2.322, 2.947, 4.010, 4.823, 5.448, 6.135, and 6.760 m from bottom of heated length) by moving the equipment during a test. The density was converted to a void fraction ($v$) using the formula: $v = \frac{(\rho_l - \rho_m)}{(\rho_l - \rho_v)}$

The report [6] presents 25 tests together with RELAP5 calculation results. Since the input parameters such as pressure, mass flow rate, power and temperature are somehow not consistent with behavior of a flow because they are not measured at the same time in 10 locations along the channel in test section but are measured in sequence during the test, then to simulate these test it is need to setup base case for simulation and to perform sensitivity analysis.

*Modeling by CTF*

Figure 2 shows the CTF modeling of BM ENTEK with 12 channels numbered from 1 to 12 at the left and 18 gaps numbered from 1 to 18 at the right. The geometry data are taken from the Ref. [6] and the initial data are taken from tests discussed in the section 4.1

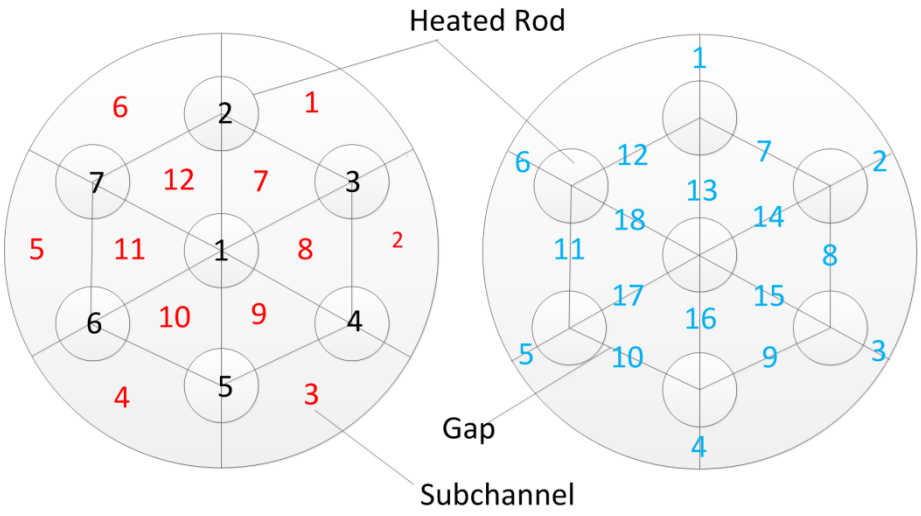


Figure 2 BM ENTEK modeling by CTF

## 4. Results and discussions

### 4.1 Setting for base case and sensitivity analysis

Tens tests are selected to study. The tests: T01, T04, T08, T10 and T14 are implemented at pressure of 3 MPa. The five other tests: T17, T18, T22, T24 and T25 are performed at pressure of 7 MPa. The input for base case is selected by the average values of input parameters measured at ten locations. The sensitivity study includes two cases for each test. The first is maximum voiding case by selection of maximum pressure, mass flow rate and minimum power and temperature measured. The second is minimum voiding case by selection of minimum pressure, mass flow rate and maximum power, temperature.

Table 1 setting for base case and sensitivity cases in according to test 01 and test 17

| Test No | P (MPa) | G (kg/s) | N (kW) | T (K) | Z (m) | Void exp |
|---|---|---|---|---|---|---|
| T01 | 3.13 | 0.4364 | 305.6 | 373 | 0.385 | 0.0 |
| | 3.16 | 0.4353 | 305.1 | 388 | 0.948 | 0.0 |
| | 3.16 | 0.4344 | 305.1 | 388 | 1.573 | 0.0 |
| | 3.11 | 0.4336 | 300.8 | 389 | 2.322 | 0.0 |
| | 3.06 | 0.4481 | 302.3 | 389 | 2.947 | 0.0 |
| | 3.13 | 0.4403 | 296.7 | 389 | 4.010 | 0.0 |
| | 3.08 | 0.4339 | 296.8 | 388 | 4.823 | 0.027 |
| | 3.11 | 0.4389 | 297.0 | 388 | 5.448 | 0.178 |
| | 3.13 | 0.4344 | 297.8 | 388 | 6.135 | 0.493 |
| | 3.09 | 0.435 | 296.0 | 388 | 6.760 | 0.635 |
| Base case | 3.12 | 0.4370 | 303 | 387 | | |
| Min void | 3.16 | 0.4389 | 296 | 373 | | |
| Max void | 3.06 | 0.4336 | 305.6 | 389 | | |
| T17 | 7.21 | 0.8956 | 308.0 | 496 | 0.385 | 0.0 |
| | 7.22 | 0.8794 | 303.1 | 498 | 0.948 | 0.004 |
| | 7.24 | 0.8797 | 302.4 | 501 | 1.573 | 0.006 |
| | 7.09 | 0.8722 | 303.3 | 494 | 2.322 | 0.0 |
| | 7.11 | 0.8825 | 301.6 | 494 | 2.947 | 0.009 |
| | 7.18 | 0.8853 | 302.1 | 496 | 4.010 | 0.002 |
| | 7.20 | 0.8781 | 301.4 | 497 | 4.823 | 0.017 |
| | 7.17 | 0.8814 | 302.0 | 497 | 5.448 | 0.033 |
| | 7.16 | 0.8822 | 301.6 | 494 | 6.135 | 0.079 |
| | 7.16 | 0.8850 | 302.2 | 493 | 6.760 | 0.194 |
| Base case | 7.17 | 0.8821 | 302.8 | 496 | | |
| Min void | 7.24 | 0.8956 | 301.4 | 493 | | |
| Max void | 7.09 | 0.8722 | 301.4 | 501 | | |

For remaining tests, the experiment data can be found in [6] and the settings base case and sensitivity cases are similar to Table 1.

### 4.2 Along channel void fraction distribution discussion

Table 2 and Table 3 show the void fraction distribution calculation results versus experiment distribution along the channel. Table 4 shows the deviation between void fraction distribution calculation results versus experiment distribution. It is observed that CTF's void fraction distribution predictions for base cases are good agreement with experiment distribution with mainly deviation around 0.03 of void. The maximum deviations with value around 0.1 are occurred just one or two locations of the tests T04 and T08. Especially, for the five tests at 7 MPa (T17, T18, T22, T24 and T25), the very good void fraction distribution calculations are agreed with experiment distribution with deviation not more than 0.03 void along the channel.

Table 2 Base case void fraction distribution calculations vs experiment distribution for cases at 3MPa.

| **Z** | **T01x** | **T01c** | **T04x** | **T04c** | **T08x** | **T08c** | **T10x** | **T10c** | **T14x** | **T14c** |
|---|---|---|---|---|---|---|---|---|---|---|
| 0.385 | 0 | 0 | 0 | 0 | 0.003 | 0 | 0 | 0 | 0.002 | 0 |
| 0.948 | 0 | 0 | 0.006 | 0 | 0.01 | 0 | 0.001 | 0 | 0.001 | 0 |
| 1.573 | 0 | 0 | 0.015 | 0 | 0.001 | 0 | 0.006 | 0 | 0 | 0 |
| 2.322 | 0 | 0 | 0 | 0 | 0 | 0 | 0 | 0 | 0 | 0 |
| 2.947 | 0 | 0 | 0.002 | 0 | 0 | 0 | 0.006 | 0 | 0 | 0 |
| 4.01 | 0 | 0 | 0.002 | 0 | 0.206 | 0.088 | 0.165 | 0.067 | 0.24 | 0.183 |
| 4.823 | 0.027 | 0.003 | 0.043 | 0.022 | 0.621 | 0.574 | 0.398 | 0.342 | 0.484 | 0.441 |
| 5.448 | 0.178 | 0.155 | 0.136 | 0.157 | 0.756 | 0.759 | 0.541 | 0.608 | 0.594 | 0.588 |
| 6.135 | 0.493 | 0.591 | 0.299 | 0.459 | 0.83 | 0.842 | 0.652 | 0.723 | 0.646 | 0.673 |
| 6.76 | 0.635 | 0.706 | 0.472 | 0.584 | 0.86 | 0.877 | 0.74 | 0.771 | 0.718 | 0.714 |

(x = Experiment, c= Calculation)

Table 3 Base case void fraction distribution calculations vs experiment distribution for cases at 7MPa.

| **Z** | **T17x** | **T17c** | **T18x** | **T18c** | **T22x** | **T22c** | **T24x** | **T24c** | **T25x** | **T25c** |
|---|---|---|---|---|---|---|---|---|---|---|
| 0.385 | 0 | 0 | 0 | 0 | 0.001 | 0 | 0 | 0 | 0 | 0 |
| 0.948 | 0.004 | 0 | 0.003 | 0 | 0.018 | 0 | 0 | 0 | 0 | 0 |
| 1.573 | 0.006 | 0 | 0 | 0 | 0.015 | 0 | 0 | 0 | 0 | 0 |
| 2.322 | 0 | 0 | 0.009 | 0 | 0.085 | 0.03 | 0 | 0 | 0 | 0 |
| 2.947 | 0.009 | 0 | 0.089 | 0.005 | 0.22 | 0.134 | 0 | 0 | 0 | 0 |
| 4.01 | 0.002 | 0 | 0.275 | 0.179 | 0.446 | 0.496 | 0.1027 | 0.076 | 0 | 0.001 |
| 4.823 | 0.017 | 0 | 0.405 | 0.381 | 0.579 | 0.616 | 0.2814 | 0.25 | 0.1548 | 0.123 |
| 5.448 | 0.033 | 0 | 0.485 | 0.503 | 0.654 | 0.694 | 0.3973 | 0.406 | 0.4021 | 0.364 |
| 6.135 | 0.079 | 0.056 | 0.553 | 0.585 | 0.733 | 0.75 | 0.4834 | 0.512 | 0.5178 | 0.591 |
| 6.76 | 0.194 | 0.17 | 0.612 | 0.628 | 0.79 | 0.781 | 0.5585 | 0.564 | 0.6398 | 0.67 |

It is found that CTF tend to under prediction when experiment void fraction below 0.2 where the CTF's modeling for normal wall flow regime map is small bubble. At the nearly outlet of the channel where the experiment data are more above 0.2, CTF tend to over prediction. Thus, CTF boiling model is still needed to be improved for both sub cooled and nucleate boiling regimes in order to generate more void in sub cooled region and reduce void at nucleate boiling region.

Table 4 Deviation between void fraction distribution calculation results versus experiment distribution

| Z | Err(T01)* | Err(T04) | Err(T08) | Err(T10) | Err(T14) | Err(T17) | Err(T18) | Err(T22) | Err(T24) | Err(T25) |
|---|---|---|---|---|---|---|---|---|---|---|
| 0.385 | 0 | 0 | 0.003 | 0 | 0.002 | 0 | 0 | 0.001 | 0 | 0 |
| 0.948 | 0 | 0.006 | 0.01 | 0.001 | 0.001 | 0.004 | 0.003 | 0.018 | 0 | 0 |
| 1.573 | 0 | 0.015 | 0.001 | 0.006 | 0 | 0.006 | 0 | 0.015 | 0 | 0 |
| 2.322 | 0 | 0 | 0 | 0 | 0 | 0 | 0.009 | 0.055 | 0 | 0 |
| 2.947 | 0 | 0.002 | 0 | 0.006 | 0 | 0.009 | 0.084 | 0.086 | 0 | 0 |
| 4.01 | 0 | 0.002 | 0.118 | 0.098 | 0.057 | 0.002 | 0.096 | 0.05 | 0.0267 | 0.001 |
| 4.823 | 0.024 | 0.021 | 0.047 | 0.056 | 0.043 | 0.017 | 0.024 | 0.037 | 0.0314 | 0.0318 |
| 5.448 | 0.023 | 0.021 | 0.003 | 0.067 | 0.006 | 0.033 | 0.018 | 0.04 | 0.0087 | 0.0381 |
| 6.135 | 0.098 | 0.16 | 0.012 | 0.071 | 0.027 | 0.023 | 0.032 | 0.017 | 0.0286 | 0.0732 |
| 6.76 | 0.071 | 0.112 | 0.017 | 0.031 | 0.004 | 0.024 | 0.016 | 0.009 | 0.0055 | 0.0302 |

* Err (T01) = ABS ($T01_C$-$T01_X$), c = calculation, x = experiment

### 4.3 Radial void distribution and turbulent mixing and void drift discussion

For radial void distribution, it is shown in Figure 3 that the higher void fraction exist inside the centric channels and lower void fraction exist in the surrounded channels.

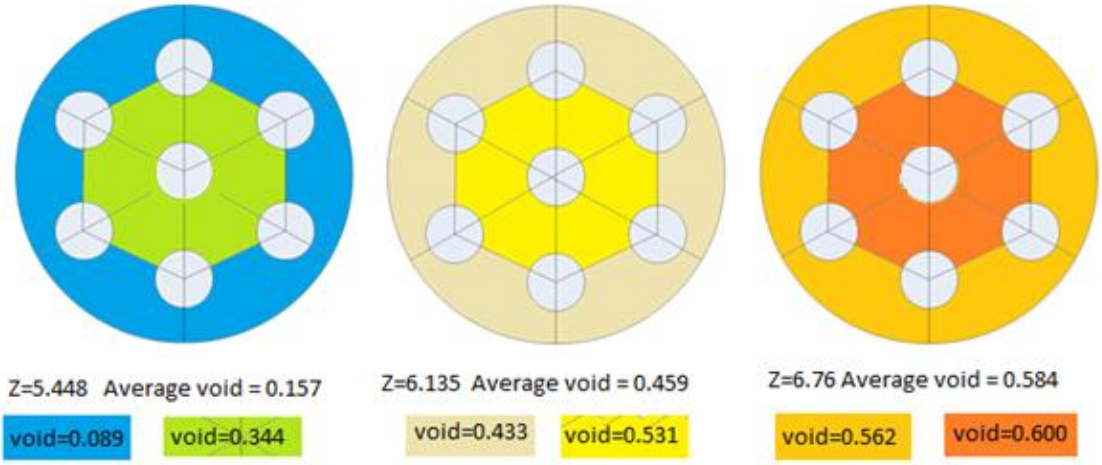


Figure 3 Radial void distribution of the test T04

The literal transportation of masses due to turbulent mixing and void drift are presented in the Ref. [8]. Based on output of CTF for total mass cross flow from channel to channel and formulas 4.168, 4.169, 4.181 and 4.182 [8], it is estimated the cross mass flows in term of flow rates caused by turbulent mixing or void drift separately for the liquid phase as in Figure 4.

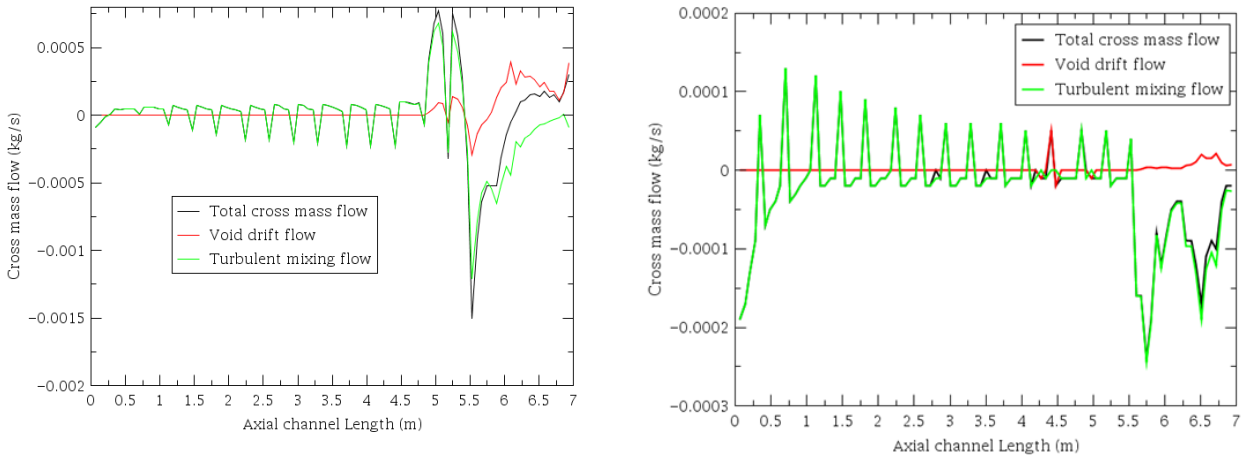


Figure 4 Cross mass flow due to turbulent mixing and void drift for test 01 (left) and test 17 (right)

It is shown that the cross transportation do not occur neither within the centric channels (channel 7 to 12) nor within surrounded channels (channel 1 to 6) but only between the surround channel and the centric channel. The literal mass transportation for void fraction is not significant in comparison with liquid transportation. The sudden change of cross flow of turbulent mixing and void drift is caused by change of heat transfer mode in one channel.

### 4.4 Sensitivity analysis discussion

As mentioned in section 4.1, two sensitivity cases with maximum and minimum voiding are setup for each test. CTF boiling modeling is assessed to be appropriate with experiment if the maximum and minimum voiding curves wrap the experiment void fraction curve and its uncertainty curves with measured accuracy of ±0.03 void. The uncertainty curves are called upper or under curves if they are derived from experiment curve with adding +0.03 or -0.03 of void, respectively. In Figure 5 and Figure 6, $T^*_{exp}$, $T^*_{max}$, $T^*_{min}$, $T^*_{Upper}$ and $T^*_{under}$ are corresponding to experiment, maximum voiding, minimum voiding, upper uncertainty (+0.03) and under uncertainty (-0.03) curves. It is obviously seen that for two tests T01 and T14 with pressure around 3MPa, the maximum and minimum voiding curves wrap experiment and its uncertainty curves as desired.

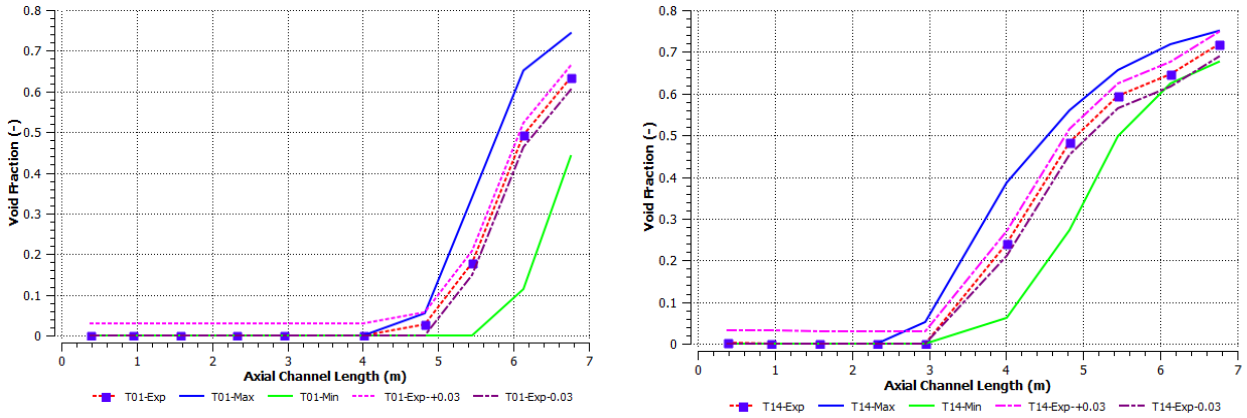


Figure 5 Maximum and minimum voiding curves versus experiment and its uncertainty curves for tests T01 and T14.

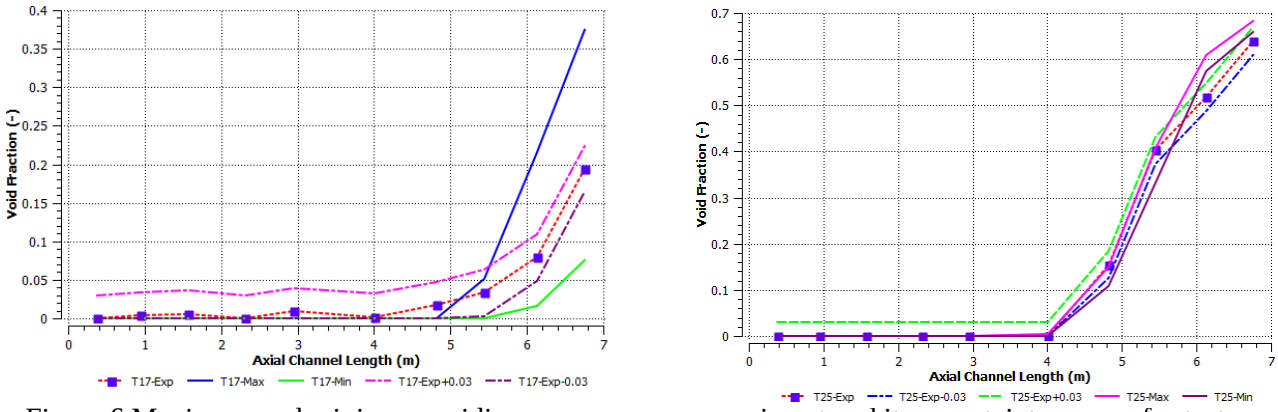


Figure 6 Maximum and minimum voiding curves versus experiment and its uncertainty curves for tests T17 and T25.

Looking at the test T25 with pressure around 7 MPa, the sensitivity curves do not wrap the experiment curves completely. In this case, the minimum voiding curve is even over the upper uncertainty curve at the downstream of the channel where the measured void fraction above 0.5. Thus, through the right graph of Figure 6, it is shown clearly that CTF gives over void prediction even in case of minimum voiding. This is due to CTF boiling models with void fraction over 0.2 tend to over prediction.

### 4.5 Propagation of the experiment uncertainty

The experiment uncertainties on the input parameters for all tests are mentioned in section 3. To investigate the experiment uncertainty, the calculations are performed with each base case for each test to get nominal void fraction distribution column, $\alpha_{nom,}$ then each parameter will be change independently to upper bound or lower bound of uncertainty to investigate the deviation of its void fraction distributions with its base cases distributions.

Table 5 Deviation of void fraction distributions on input parameter uncertainties versus nominal void fraction and experiment distributions for test T01

| Z | T01x | T01b | T01P+ | T01P- | T01G+ | T01G- | T01N+ | T01N- | T01T+ | T01T- |
|---|---|---|---|---|---|---|---|---|---|---|
| 0.385 | 0 | 0 | 0 | 0 | 0 | 0 | 0 | 0 | 0 | 0 |
| 0.948 | 0 | 0 | 0 | 0 | 0 | 0 | 0 | 0 | 0 | 0 |
| 1.573 | 0 | 0 | 0 | 0 | 0 | 0 | 0 | 0 | 0 | 0 |
| 2.322 | 0 | 0 | 0 | 0 | 0 | 0 | 0 | 0 | 0 | 0 |
| 2.947 | 0 | 0 | 0 | 0 | 0 | 0 | 0 | 0 | 0 | 0 |
| 4.01 | 0 | 0 | 0 | 0 | 0 | 0 | 0 | 0 | 0 | 0 |
| 4.823 | 0.027 | 0.003 | 0.002 | 0.008 | 0.002 | 0.002 | 0.008 | 0.002 | 0.009 | 0.002 |
| 5.448 | 0.178 | 0.155 | 0.131 | 0.181 | 0.143 | 0.143 | 0.177 | 0.133 | 0.181 | 0.131 |
| 6.135 | 0.493 | 0.591 | 0.578 | 0.604 | 0.584 | 0.584 | 0.602 | 0.579 | 0.602 | 0.579 |
| 6.76 | 0.635 | 0.706 | 0.698 | 0.713 | 0.702 | 0.702 | 0.712 | 0.699 | 0.712 | 0.699 |

(x=experiment, b= base case, P±, G±, N±, T± = pressure, mass flow rate, power and temperature changed)

Table 5 and Figure 7 show the deviation of void fraction distribution results from nominal void fraction distribution due to change of input parameter for test T01. Thus, it is observed that the uncertainty cases are not significant discrepancy with base case.

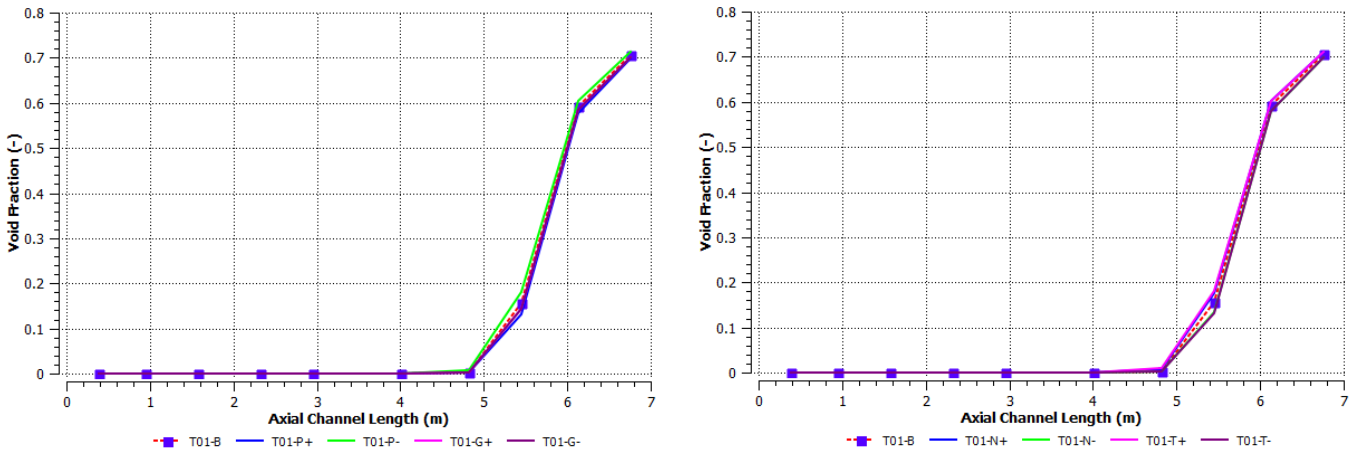


Figure 7 Uncertainty void fraction distributions for test T01

Table 6 shows the maximum deviation compared in 10 measured locations along the channel between nominal void fraction distribution and void fraction distributions for each change on input parameters with the tests: T01, T08, T17 and T25. It is observed that the change of pressure and temperature is more sensitive than mass flow rate and power, except case of T01.

Table 6 Maximum deviation of void fraction distribution on input parameters versus base case for tests: T01, T08, T17 and T25

| | Z (m) | T01 | Z (m) | T08 | Z (m) | T17 | Z (m) | T25 |
|---|---|---|---|---|---|---|---|---|
| Pressure ±1.5% | 5.448 | $\alpha_{nom}$ ± 0.026 | 4.823 | $\alpha_{nom}$ ± 0.014 | 6.76 | $\alpha_{nom}$ ±0.03 | 5.448 | $\alpha_{nom}$ ±0.028 |
| Inlet Temp ± 1K | 5.448 | $\alpha_{nom}$ ± 0.026 | 4.823 | $\alpha_{nom}$ ± 0.012 | 6.76 | $\alpha_{nom}$ ±0.023 | 5.448 | $\alpha_{nom}$ ±0.02 |
| Mass flow rate ± 0.0018 kg/s | 5.448 | $\alpha_{nom}$ ± 0.012 | 4.823 | $\alpha_{nom}$ ±0.01 | 6.76 | $\alpha_{nom}$ ±0.004 | 5.448 | $\alpha_{nom}$ ±0.005 |
| Power ± 2kW | 5.448 | $\alpha_{nom}$ ± 0.022 | 4.823 | $\alpha_{nom}$ ±0.01 | 6.76 | $\alpha_{nom}$ ±0.012 | 5.448 | $\alpha_{nom}$ ±0.008 |

In overall, it is concluded that the deviations between nominal void fraction distribution and its void fraction distributions due to uncertainties of measured input parameter are within measured void fraction accuracy (± 0.03). So that, CTF boiling models is stable enough with uncertainty from measured input parameters.

## 5. Conclusions

It is summarized some assessment of CTF boiling model for ENTEK BM tests as following:

- CTF give void fraction distribution predictions for most all base cases are good agreement with experiment distributions with mainly deviation within experiment measured accuracy for void fraction (0.03 of void) and the maximum deviations with 0.1 of void between CTF prediction and experiment occur at downstream of channel in some tests.
- CTF boiling model tend to under predict void fraction in sub cooled region where void fraction below 0.2 and tend to over predict void fraction at nucleate boiling region where void fraction above 0.2.
- The deviations between nominal void fraction distribution and its void fraction distributions due to uncertainties of measured input parameter are within measured void fraction accuracy (± 0.03) and CTF boiling model is rather sensitivity with the change of pressure and inlet temperature than change of power and mass flow rate based on experimental measured accuracy.
- Turbulent mixing and void drift effects occur only between surrounded channels and centric channels and the sudden change of cross mass flow of liquid phase happens due to change of heat transfer mode in one channel.
- Finally, CTF can simulate ENTEK BM tests with the appropriate results.

**Acknowledgment:** The authors of this paper wish to express their appreciation for the financial support from Ministry of Science and Technology (MOST) through the National R&D Project: "Study the Nuclear Power Plant's Technology proposed for Ninhthuan 1 and Ninhthuan 2 in order to support Basic Design's Review", code KC.05.26/11-15. The authors of this paper also wish to express their appreciation to Mr. Duong Quoc Hung, Ph.D. for his exchange information of CTF training between Vietnam Agency for Radiation and Nuclear Safety (VARANS) and Pennsylvania State University (PSU).

## Nomenclature

| | | | |
|---|---|---|---|
| EPRI | Electric Power Research Institute | PSBT | PWR Sub-channel Bundle Tests |
| TPTF | Two Phase Test Facility | ENTEK BM | BM facility at ENTEK |
| $\dot{m}_k^{TM}$ | Mass exchange of phase k (kg/m$^2$.s) | $\beta_{TP}$ | Two phase turbulent mixing coefficient |
| $\dot{m}_k^{VD}$ | Mass exchange due to drift model (kg/s) | $\bar{\rho}$, $\rho_m$ | Mixing density (kg/m$^3$) |
| $h_{g,sat}$ | Vapor saturation enthalpy (J/kg) | $\rho_{ki}$ | Density of phase k in sub channel i (kg/m$^3$) |
| $h_{int,shl}$ | Super-heated liquid interface heat transfer coefficient (W/m2.K) | $\rho_l$ | Liquid density (kg/m$^3$) |
| $h_{int,shv}$ | Super-heated vapor interface heat transfer coefficient (W/m2.K) | $\rho_v$ | Vapor density (kg/m$^3$) |
| $h_{int,scl}$ | Sub-cooled liquid interface heat transfer coefficient (W/m2.K) | $\Delta X$ | Mesh-cell axial height (m) |
| $h_{int,scv}$ | Sub-cooled vapor interface heat transfer coefficient (W/m2.K) | $A_s$ | Conductor surface area in mesh cell (m$^2$) |
| $h_{l,sat}$ | Liquid saturation enthalpy (J/kg) | $A_x$ | Mesh-cell area, X normal (m$^2$) |
| $A'''_{int,shl}$ | Super-heated liquid interfacial area per unit volume (m$^{-1}$) | $C_{pl}$ | Liquid specific heat, constant pressure (J/kg.K) |
| $A'''_{int,shv}$ | Super-heated vapor interfacial area per unit volume (m$^{-1}$) | $C_{pv}$ | Vapor specific heat, constant pressure (J/kg.K) |
| $A'''_{int,scl}$ | Sub-cooled liquid interfacial area per unit volume (m$^1$) | hc | Chen correlation heat transfer coefficient (W/m$^2$.K) |
| $A'''_{int,scv}$ | Sub-cooled vapor interfacial area per unit volume (m$^1$) | hg | Vapor enthalpy (J/kg) |
| $\bar{G}$ | Mixing mass flux (kg/m$^2$.s) | $H_l$ | Liquid enthalpy (J/kg) |
| $\alpha_{ki}$ | Void fraction of phase k induced by sub channel i | Tcrit | Critical heat flux temperature (K) |
| $\alpha_{kiEQ}$ | Equilibrium quality void fraction | $T_l$ | Liquid temperature (K) |
| Sk | Gap width between channels i and j (m) | $\Gamma'''$ | Volume metric mass flow rate (kg/m3.s) |

**References**

[1] M.Gluck, "Validation of the sub-channel code F-COBRA-TF, Part II Recalculation of void measurements", Nuclear Engineering and Design 238 (2008) 2317–2327.

[2] J. Michael Doster, "Assessment of the Performance of COBRA-TF for the Prediction of Subcooled Boiling Conditions in Rod Bundles", CASL-8-2013-0201-000, September 30, 2013.

[3] M. Avramova, A. Velazquez-Lozada, and A. Rubin., "Comparative Analysis of CTF and Trace Thermal-Hydraulic Codes Using OECD/NRC PSBT Benchmark Void Distribution Database", Hindawi Publishing Corporation, Science and Technology of Nuclear Installations, Volume 2013, Article ID 725687. Accepted 16 November 2012, pp. 2-5.

[4] Murray Cameron Thames., "Application and Assessment of a 9-equation Sub channel Methodology to Rod Bundles", A thesis in Nuclear Engineering for the Degree of Master of Science, North Carolina State University, 2014, pp. 44, 55.

[5] Robert K. Salko., "Improvement of COBRA-TF for modeling of PWR cold- and hot-legs during reactor transients", A dissertation in Nuclear Engineering for the Degree of Doctor of Philosophy, The Pennsylvania State University, May 2012, pp. 7-17.

[6] P. L. Garner., "RELAP5/MOD3.2 Analysis of INSC Standard Problem INSCSP-R7: Void Fraction Distribution over RBMK Fuel Channel Height for Experiments Performed in the ENTEK BM Test Facility", United States International Nuclear Safety Center, Reactor Analysis and Engineering Division, Argonne National Laboratory, April 2002, pp. 6-9.

[7] S. G. Beus, "A two-phase turbulent mixing model for flow in rod bundles," Tech. Rep. WAPD-T-2438, Bettis Atomic Power Laboratory, 1970.

[8] Robert K. Salko, Maria N. Avramova, "CTF Theory Manual", The Pennsylvania State University, March 10, 2015, pp 29-131.